Available online at www.sciencedirect.com
ScienceDirect
Journal of Terramechanics 44 (2007) 275–291
Journal of Terramechanics
www.elsevier.com/locate/jterra

# Velocity effect of vehicle rolling resistance in sand

Barry Coutermarsh

*US Army Engineer Research and Development Center (ERDC), Cold Regions Research and Engineering Laboratory (CRREL), 72 Lyme Road, Hanover, NH 03755, United States*

Available online 24 April 2007

**Abstract**

Vehicle rolling resistance is important to vehicle and aircraft ground movement in loose soil and sand conditions, especially in military operations. Off-road rolling resistance measurements have been taken at relatively low velocities, 2.1–4.6 m/s (meters per second) (7–15 ft/s) (4–9 knots), which has precluded studying any potential velocity effect on rolling resistance. With the emergence of aircraft designed to be used on unimproved soil runways and the military's proposed new vehicles, especially the lighter-weight, 23–500-kg (50–1100-lbs) robotics, capable of high-velocity off-road movement, it is important that the rolling resistance be measured at velocities closer to the expected operating conditions. This paper presents data from rubber tire rolling resistance measurements in three depths of uniform-density dry sand at velocities from 2.1 up to 18 m/s (7–58 ft/s) (4–34 knots) and three load ranges from 4534 to 10,266 N (1020–2308 lbs). In dry sand the rolling resistance increases with velocity until the tire starts to "plane," where it levels off or decreases and it is modified by load. Limited past work in this area is presented along with some existing analytical descriptions of rolling resistance versus velocity. Limited agreement between the published equations and the test data, along with contradictory published results, indicate that additional work on this topic is needed.


*Keywords:* Rolling resistance; Vehicle rolling resistance; Aircraft rolling resistance; Vehicle mobility in sand

## 1. Introduction

CRREL has studied ground vehicle performance under summer off-road conditions at velocities up to 21 m/s (68 ft/s) (40 knots) and aircraft ground performance from unimproved runways to determine the increased drag the vehicle or aircraft experiences traveling on a soft sand surface. To design vehicles, simulate their movement in virtual scenarios, or determine operating parameters, this loose surface drag needs to be accurately accounted for.

This drag has been referred to by various names and is expressed here as a rolling friction factor (RFF):

$$\mathrm{RFF} = F_{\mathrm{D}}/L \tag{1}$$

where $F_{\mathrm{D}}$ is the drag force on the tire and $L$ is the vertical load.

Rolling resistance measurements on snow or soil surfaces were frequently taken at low velocity, 0.1–5.5 m/s (0.25–18 ft/s) (4–11 knots) [1–4], both in the laboratory and in field experiments. With the increased use of aircraft on unimproved runways, limited studies were performed to quantify the effect that wheel velocity had on drag at velocities up to about 61 m/s (200 ft/s) (120 knots) with a more controlled body of work for the effect of a tire rolling through clay or sand [5,7,9].

All-weather combat vehicles and robotics capable of higher-than-traditional off-road velocities are of interest, and it is instructive to determine the relationship between velocity and drag in a range lower than found in aircraft take-off velocities.

Furthermore, for military computer simulations to become more accurate in predicting vehicle movement across varied terrain there is a need for better rolling resistance characterizations at ground vehicle speeds. The measurements described in this paper are a step in a controlled

*E-mail address:* Barry.A.Coutermarsh@erdc.usace.army.mil

0022-4898/$20.00 
doi:10.1016/j.jterra.2007.03.001

and focused look at the RFF of tires across a loose sand surface at ground vehicle velocities.

## 2. Background

### 2.1. Sand drag

Past work in soil drag experiments was researched to find comparative data to the sand experiments in the test velocity range presented in this report of 2.1–15.5 m/s (7–51 ft/s) (4–30 knots). The largest body of work found was tire drag through fine-grained soils (clay) with limited sand experiments. Much of the analysis done was on data collected from single-wheel tests performed at the NASA Langley Landing Loads Track in Hampton, Virginia, in the late 1960s and early 1970s. In those tests [5,6] a $29 \times 11.0$–10 8 PR Type III flotation tire at three pressures, 207 kPa (30 psi), 310 kPa (45 psi), and 483 kPa (70 psi), with a 22-kN (5000-lb) load was run through "buckshot" clay and sand from Newport News, Virginia. The tire had a nominal diameter of 0.74 m (29 in.) and a maximum cross sectional width of 0.28 m (11 in.). The tire hard-surface footprints measured at a load of 19 kN (4200 lb) varied with pressure as follows: 207 kPa (30 psi)–0.0777 $m^2$ (120 $in.^2$), 310 kPa (45 psi)–0.0559 $m^2$ (87 $in.^2$), and 483 kPa (70 psi)–0.0381 $m^2$ (59 $in.^2$). Tire velocity varied from 0 to 48.8 m/s (0–160 ft/s) (0–95 knots). The sand was classified as poorly graded with 6–8% moisture content and compacted to 1666 kg/$m^3$ (104 lb/$ft^3$) with a surface CBR of 1.5 and a gradient of 1 CBR unit per inch of depth.

A 1975 study [7] in the United Kingdom investigated tire drag using a heavy load friction vehicle (HLFV) with a 276 kPa (40 psi ), $32 \times 10.00 - 15$ Meteor tire in dry Leighton Buzzard best dried 'A' sand. These two studies, along with other analysis done on these studies, are compared in the discussion of our results. Where the studies used multiple loads, tire pressures, or sizes, we focused on the results from the parameters closest to our experiments.

Finally, there is a synopsis by the US Army Corps of Engineers on rolling friction for aircraft taking off on unpaved runways [8]. Various analytical relationships are discussed in that report, some of which will be compared with our sand drag data.

The previous work generally treated the soil as a homogenous material in depth. The tire creates a rut to a depth determined by the physics of the tire and soil. This study adds the effect that a sand of finite depth underlain by a competent layer has on rut development.

The variables we wanted to look at closely were material depth, rut depth, velocity, drag force, and load. Following past work, we plot the rut depth in the form of a sinkage ratio ($Z/D$) by dividing the rut depth ($Z$) by the unloaded wheel diameter ($D$).

### 2.2. Experimental design

Our sand drag experiments were performed at NASA Langley in Hampton, Virginia, using the NASA Langley Instrumented Tire Test Vehicle (ITTV). The experiments were designed to measure the rolling resistance of a single tire at three loads in three depths of sand over four velocities. Table 1 presents the nominal test matrix. Each material depth and load was performed across the listed velocity range, resulting in a total of 36 tests. The constraints of the testing area dictated that only the velocity and load parameters could be randomized within each material depth.

### 2.3. Material

The material used was a dry (average 1% moisture content) mortar sand at an average density of 1272 kg/$m^3$ (79 pcf). It was placed at depths of 0.0508, 0.127, and 0.1778 m (2, 5, and 7 in.). Cone Index (CI) values were determined in the laboratory with a 0.000323-$m^2$ basal area (0.50-$in.^2$) cone and by averaging 12 tests. Table 2 lists the CI values obtained.

### 2.4. Tire

The tire used was a Goodyear Wrangler HT 235/75 R15 at 241 kPa. The tire has an unloaded overall diameter of 0.7330 m (28.85 in.) and a section width of 0.235 m (9.25 in.). Table 3 lists the tire footprint dimensions at loads close to those used in the tests. The tire footprints are more oval shaped than rectangular but a representative width and length are listed in the table for reference. The

Table 2
Cone index values for the sand

| Depth (m) | CI (psi) | CI (kPa) |
|---|---|---|
| 0 | 0 | 0.0 |
| 0.025 | 7.1 | 48.8 |
| 0.051 | 15.2 | 104.5 |
| 0.076 | 26.9 | 185.7 |
| 0.102 | 39.9 | 274.8 |
| 0.127 | 53.9 | 371.4 |
| 0.152 | 66.9 | 461.0 |
| 0.178 | 76.7 | 528.8 |
| 0.203 | 84.5 | 582.6 |
| 0.229 | 92.0 | 634.4 |
| 0.254 | 83.5 | 575.6 |

Table 1
Test matrix for the sand experiments

| Nominal velocity (ft/s) | Nominal velocity (m/s) | Material depth (in.) | Material depth (m) | Average load (lb) | Average loads (N) |
|---|---|---|---|---|---|
| 7, 15, 29, 51 | 2.1, 4.6, 8.8, 15.5 | 2, 5, 7 | 0.0508, 0.127, 0.1778 | 1020, 1700, 2308 | 4534, 7569, 10,266 |

Table 3
Goodyear Wrangler 235/75 R15 tire hard-surface footprint dimensions at 241 kPa and three loads near the average test loads

| Load | | Footprint width | | Footprint length | | Footprint area | |
|---|---|---|---|---|---|---|---|
| (lb) | (N) | (in.) | (m) | (in.) | (m) | ($in.^2$) | ($m^2$) |
| 981 | 4364 | 6 | 0.1524 | 6.2 | 0.1575 | 18.6 | 0.0120 |
| 1801 | 8011 | 6.1 | 0.1549 | 8.2 | 0.2083 | 32.7 | 0.0211 |
| 2672 | 11,886 | 6.4 | 0.1626 | 10.5 | 0.2667 | 53.2 | 0.0343 |

footprint areas were calculated by planimeter from an inked imprint of the footprint on a hard surface.

### 2.5. Test vehicle

The ITTV is a 173.5-kN (19.5-ton) Ford CT 900 truck with pneumatic cylinders on the rear, where a test tire can be mounted, as shown in Fig. 1.

The test tire tracks between the truck wheels thus avoiding following in the ruts made by the truck tires. Different loads, up to 22.2 kN (5000 lb), can be applied by using the pneumatic cylinders to lower the tire to the surface. The various forces on the tire are measured by strain gage beams mounted around the top of the cylinders.

### 2.6. Test location

The test area on the NASA Langley grounds was a straight, level, asphalt-paved road with a concrete test section containing a 0.127-m deep × 1.0668-m wide × 30.5-m (5-in. × 3.5-ft × 100-ft) long trench. The 0.0508-m (2-in.) depth sand was laid on the concrete surface over a 1.0668-m-wide × 30.5-m-long (3.5-ft × 100-ft) area. Since the pneumatic cylinder holding the test tire on the ITTV had a limited vertical lift capability, the two test sequences using the deeper sand depths had to be run by placing the sand in the trench. The surface of the 0.1778-m (5-in.) depth was level with the surrounding concrete, and the surface of the 0.127-m (7-in.) depth was left about 0.0508 m (2 in.) above the concrete surface.

Fig. 1. NASA ITTV with mounted test tire.

### 2.7. Test procedure

Each test sequence followed the same general procedure. The sand was raked and leveled before each test run. The ITTV was prepared for each test at the beginning of the road section by lowering the test tire to the surface to apply the vertical load. After the first test with the sand 0.0508-m deep (2-in.) over the concrete surface, it was realized that the load on the test tire increased when it entered the test section because the added height of the sand forced the test tire higher, supporting more of the truck weight. Applying a lighter load than desired during the setup compensated somewhat for this, but since the pneumatics did not allow

Fig. 2. Rut profile measurement.

Table 4
Load range number, mean, and standard error

| Load range number | Range mean load (lb) | Standard error | Range mean load (N) | Standard error |
|---|---|---|---|---|
| 1 | 1020 | 43 | 4534 | 193 |
| 2 | 1700 | 57 | 7569 | 254 |
| 3 | 2308 | 39 | 10,266 | 173 |

for precise adjustments, the load consequently varied both from the nominal and between tests. It was also discovered as the velocity increased that the rut depth changed, as will be discussed later, and this effect caused the load to vary from the desired load. Because of the above variability in load, we describe the loads as three load ranges as listed in Table 4.

After setup the ITTV accelerated to the target velocity and entered the test section, with the test tire steered down the center of the sand. Measurements were collected at 100 Hz and averaged during post-processing to arrive at the drag and load readings for each test.

The rut depths and profiles were measured after each test run by the following procedure. A thin metal sheet with paper taped to it was inserted into a representative section of rut. Paint was sprayed on the paper following the upper rut surface laterally out to the undisturbed sand at the side of the rut, as shown in Fig. 2. The resulting profile showed the rut width and depth and also profiled the material displaced by the tire to each side. The rut depth is defined as the distance from the undisturbed sand surface to the bottom of the rut, as shown in Fig. 3. The displaced sand data have not been analyzed for this paper, but the hope is that they will provide insight into the kinetic energy being imparted to the sand by the tire passage.

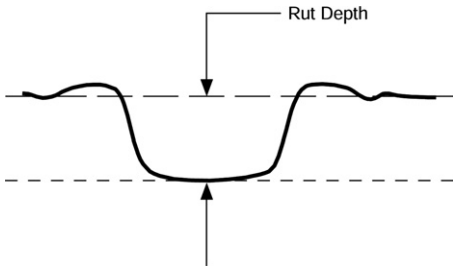


Fig. 3. Rut depth description.

## 3. Results

Fig. 4 shows $Z/D$ versus velocity for each material depth by load range. As mentioned previously the results are

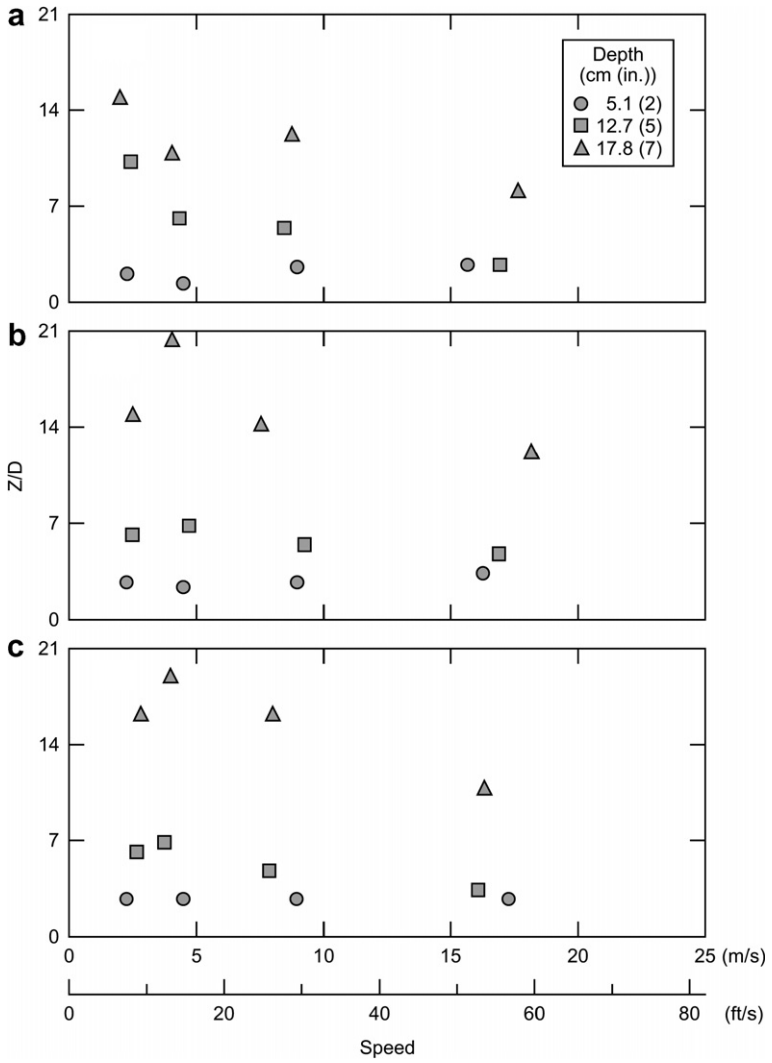


Fig. 4. $Z/D$ versus speed for load range 1, 2 and 3, (a), (b) and (c), respectively.

plotted in the form of a sinkage ratio ($Z/D$) to relate to past work. In the tests presented here with only one tire diameter $D$, the sinkage ratio and rut depth are essentially equivalent varying only be a constant of $1/D$. In the lowest load range (Fig. 4a), the sinkage ratio is decreasing with increasing velocity in all but the 0.0508-m (2-in.) deep sand, where it is fairly level across the velocity range. In fact, for all the load ranges, in the 0.0508-m (2-in.) deep sand, $Z/D$ is either level or slightly increasing with velocity. In the highest two load ranges for the 0.127-m (5-in.) deep and 0.1778-m (7-in.) deep sand, $Z/D$ has a peak value somewhere between 3.6 and 7.6 m/s (11.8 and 25 ft/s) (7–15 knots) and then decreases with increasing velocity.

The RFF values for the three load ranges are presented in Fig. 5. The 0.0508-m (2-in.) deep RFF versus velocity data again show a nearly level characteristic, similar to the $Z/D$ data. In load ranges 1 and 2 these data show a very slight decrease, while in load range 3 they show a very slight increase with velocity. However, since the difference is slight, caution should be exercised in that interpretation. It is evident that the data for the two higher depths have much different RFF values from the 0.0508-m (2-in.) depth, both in magnitude and general shape of the curves. Generally speaking, the 0.0127-m (5-in.) depth RFF values peak earlier than the 0.1778-m (7-in.) depth data. The one possible exception is in load range 1, where the 0.1778-m (7-in.) deep RFF values does not exhibit a peak per se. They are fairly level with velocity from 2.6 m/s to about 10.4 m/s (8.5–34 ft/s) (5–20 knots), and at some velocity after that they start to decline.

An analysis of variance of the data shows there is a statistically significant difference (at the 95% level) between the RFF values of all three depths at load range 1 and load range 2. However, at load range 3 there is only a significant difference between the 0.0508 m (2 in.) deep data and the two greater depths. There is no significant difference between the 0.127-m (5-in.) depth and the 0.1778-m (7-in.) depth RFF values. Fig. 6 shows the RFF data on one plot grouped by load and depth. Here the difference by depth is more evident.

Although the RFF values from the two upper depths are similar, there is still a statistically significant difference

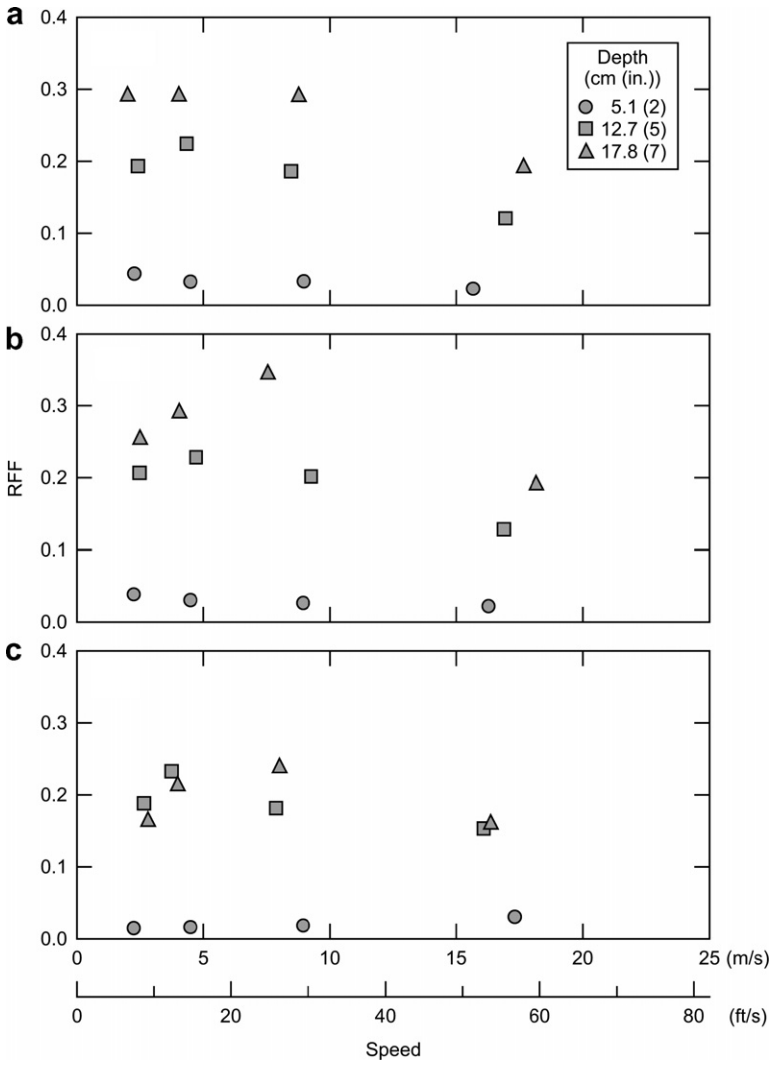


Fig. 5. RFF versus velocity for load range 1, 2 and 3, (a), (b) and (c), respectively.

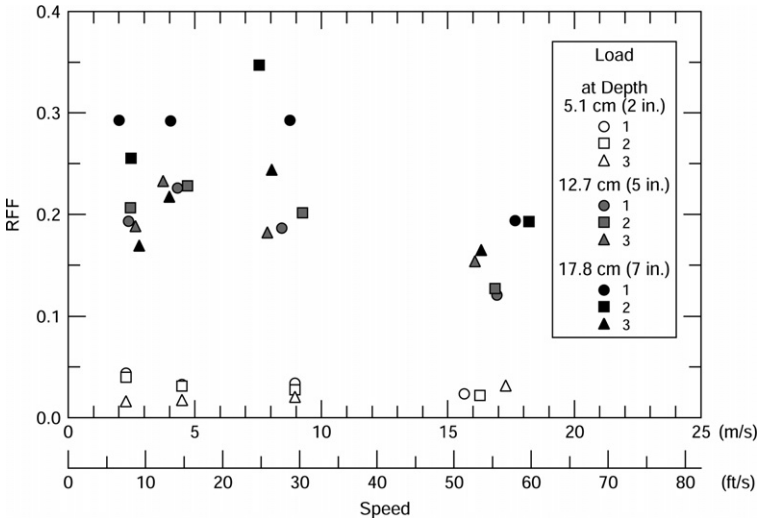


Fig. 6. RFF versus velocity for all depths and loads.

overall. As pointed out above, this is most influenced by the two lower load ranges, since load range 3 does not have a significant difference between the two upper depths. The rut depth values are plotted against RFF for each overall sand depth in Fig. 7. It is evident that the RFF generally increases with increasing rut depth at the two higher sand

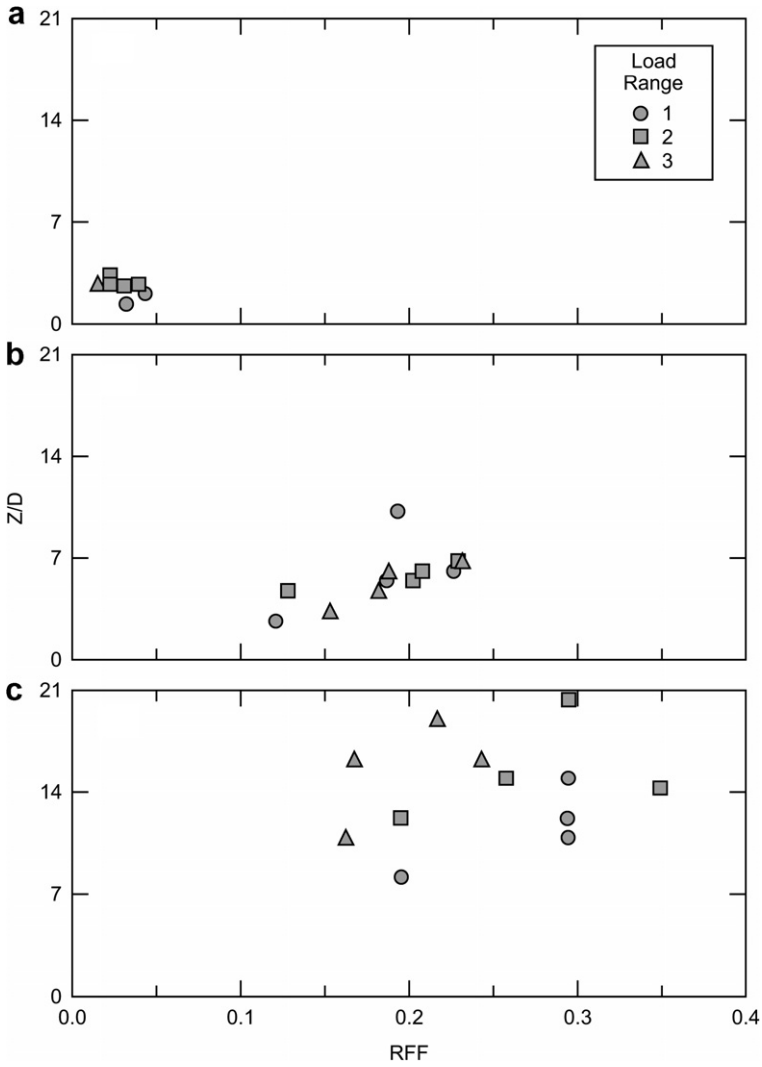


Fig. 7. Sinkage ratio versus RFF for three sand depths, (a) 0.0508 m (2 in.), (b) 0.127 m (5 in.) and (c) 0.1778 m (7 in.).

Fig. 8. Slow-speed tire traversing the 0.127 m (5 in.) deep sand.

depths, with more scatter obvious at the 0.1778-m (7-in.) sand depth.

## 4. Discussion

The sinkage ratio versus velocity data appear to show the effect of the overall sand depth. A rut cannot develop as deeply in the 0.0508-m (2-in.) deep sand, where the solid substrate is near regardless of the load. The concrete surface was used to minimize the effect of subgrade deflection so the results would predominately reflect the effect of the sand. The 0.127-m (5-in.) and 0.1778-m (7-in.) depths allow a rut to develop more, although from these data it can be seen the 0.1778-m (7-in.) deep sand has substantially deeper ruts at the lower velocities than the other two depths. As the velocity increases, this difference decreases, which implies a velocity effect. Our data show that rut depth increases across the lowest velocities, reaches a peak, and then decreases with increasing velocity at all but the lowest sand depth.

A qualitative observation was made by watching the tire traverse the sand during the tests. At the low velocities a "bow wave" was clearly visible in front of the tire, and material was pushed up in a plowing effect around the tire, as shown in Fig. 8. As the velocity increased, this wave diminished until either none or a very small one was apparent at the highest velocities. This implies a dynamic strain rate effect to the bearing capacity of the sand such that there was a velocity at which the tire was not plowing the sand as much as it was floating on the top of it. Crenshaw [9] labels this soil lift and states it is analogous to hydroplaning lift of a tire on water. Beaty [7] references a report that states that the planing velocity for sand is

$$V_p = 1.2p \tag{2}$$

where $V_p$ is the planing velocity in ft/s and $p$ is the tire pressure in psi. For our tire, this would predict the planing velocity to be

$$V_p = 1.2(35) = 42\ \text{ft/s} = 12.8\ \text{m/s}\ (25\text{knots}). \tag{3}$$

Our suspected planing velocity was somewhere between 8.2 and 15.2 m/s (27 and 50 ft/s) (16–30 knots).

This effect is mirrored somewhat in the RFF data, where the rolling resistance decreases with increasing velocity and appears to be at least partly related to the sinkage ratio. However, at the higher velocities there was more kinetic energy imparted to the sand in the form of spray, as shown in Fig. 9, which could increase the RFF also.

Fig. 7 shows the sinkage ratio, which in our study is essentially rut depth, versus RFF. The scatter at each load range, especially evident in Fig. 7c, appears to be caused by the relationship between RFF and both velocity and rut depth. If the RFF depended only on rut depth, we would theoretically see a much clearer relationship between RFF and $Z/D$ at each load. Since there is a component of RFF that is velocity dependent, this decrease in rut depth does not necessarily decrease the RFF.

Past work has also implied the existence of this phenomenon but not necessarily clearly. In [6] the sand rut depth versus velocity traces are complex and quite different for each tire pressure. The general shape of the 483-kPa

Fig. 9. Tire with spray formed at higher speeds.

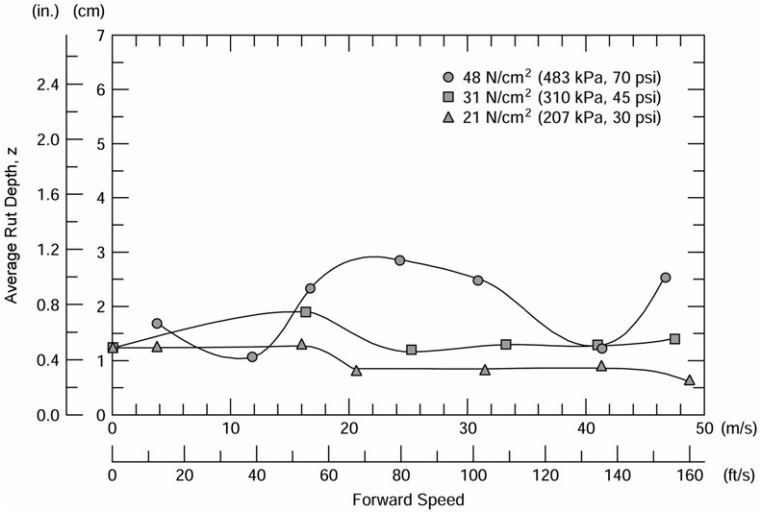


Fig. 10. General shape of the rut depth versus velocity curves from Leland [6].

(70-psi) tire's rut depth versus velocity curve is shown in Fig. 10. It decreases from about 4.7 m/s to 14.8 m/s (13.5–42.2 ft/s) (8–25 knots), where it steeply increases to about 23.2 m/s (76 ft/s) (45 knots), levels briefly, decreases to 41.2 m/s (135 ft/s) (80 knots), and then steeply increases to 48.9 m/s (160 ft/s) (95 knots). This tire pressure was much higher than our 241-kPa (35-psi) tire pressure, but its footprint area was closest to our load range 2 area, theirs being 0.0381 $m^2$ (59 $in.^2$) and ours being 0.0295 $m^2$ (45.7 $in.^2$). Their tire's diameter was 0.74 m (29 in.), which was close to our 0.733-m (28.9-in.) diameter. Their 310-kPa (45-psi) tire's rut depth gradually increases from about 0 to 18 m/s (0–59.1 ft/s) (0–35 knots), moderately decreases to about 25.7 m/s (84.4 ft/s) (50 knots), and then slowly increases slightly to about 48.9 m/s (160 ft/s) (95 knots). This general shape is similar to our 0.1778-m (7-in.) deep data, but ours peaks somewhere between 4.6 and 10.4 m/s (15 and 34 ft/s) (9–20 knots), whereas theirs peak at around 18 m/s (59.1 ft/s) (35 knots). In our data the rut depth peak had a weak trend of shifting towards higher velocity with increasing sand depth at the two highest load ranges and we could discern no effect of load on the location of the peak. Their 207-kPa (30-psi) tire's rut depth is uniform from 0 to about 15.4 m/s (0–50.6 ft/s) (0–30 knots), where it decreases steeply to about 20.6 m/s (67.5 ft/s) (40 knots) and remains fairly level up to 48.9 m/s (160.3 ft/s) (95 knots). This tire pressure is the closest to our 241-kPa (35-psi) tire pressure. We showed a similar trend in our 0.1778-m (7-in.) deep sand at the lightest load range, which may imply a flotation effect from a low ground pressure tire. In this previous work, rut depth generally decreased with deceasing tire pressure.

Also in [6], their sand RFF versus velocity curve of the highest pressure tire mimics the rut depth curve in general shape. The 310-kPa (45-psi) tire's RFF gradually decreases from 0 to about 7.7 m/s (0–25.3 ft/s) (0–15 knots), rises until about 18 m/s (59.1 ft/s) (35 knots), decreases to around 33.4 m/s (109.7 ft/s) (65 knots), increases slightly to about 41.2 m/s (135 ft/s) (80 knots), and decreases again until 48.9 m/s (160.3 ft/s) (95 knots). The 207-kPa (30-psi) tire RFF has a very gradual decrease from 0 to about 5.1 m/s (0–16.9 ft/s) (0–10 knots), where it gradually increases to about 10.3 m/s (33.8 ft/s) (20 knots) and remains fairly constant with just a small rise as the velocity increases to 48.9 m/s (160.3 ft/s) (95 knots). Our data never exhibited a clear tendency of decreasing RFF at the initial velocities, with the possible exception of the 0.0508-m (2-in.) deep sand, which, as mentioned before, is so slight as to be of questionable significance. Fig. 11 shows the general shape of the RFF versus velocity curves from Leland [6].

Between 0 and 18 m/s (0–59.1 ft/s) (0–35 knots) the RFF for their 207-kPa (30-psi) tire is about 0.07, and the highest RFF is about 0.09 at about 30.9 m/s (101.3 ft/s) (60 knots). Their highest RFF for the 483-kPa (70-psi) tire was about 0.17 at about 23.2 m/s (76 ft/s) (45 knots). The one value they had for this tire in our velocity range was about 0.08 at about 11.3 m/s (37.1 ft/s) (22 knots). The highest RFF value we obtained from this study was 0.35, obtained at load range 2 in the 0.1778-m (7-in.) deep sand at 7.3 m/s (24 ft/s) (14 knots). Their RFF generally decreases with decreasing tire pressure, which could occur because the footprint area of their tire increased with the lower air pressures.

A later study [10] that analyzed the data from [5,7] concluded that the variability might not be statistically significant and that it could account for some of the peaks in their RFF versus velocity curves. It further stated that the increase in RFF with velocity was the result of tire internal resistance with velocity rather than any soil strain rate effect, which would tend to decrease rut depth. Our data, as can be seen in the above figures, does seem to have a strain rate effect because of the decrease in rut depth with increasing velocity.

A 1975 study [7] in the United Kingdom investigated tire drag using a heavy load friction vehicle (HLFV) with a 27-kPa (40-psi), $32 \times 10.00$–15 Meteor tire in dry Leighton

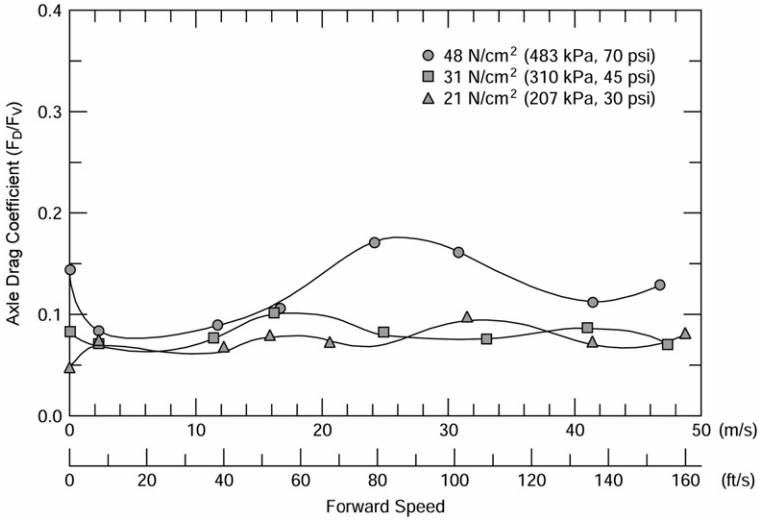


Fig. 11. General shape of the RFF versus velocity curves from Leland [6].

Buzzard best dried 'A' sand. The sand was in a 0.76-m wide × 21-m long × 0.46-m deep (2.5-ft × 69 ft × 1.5-ft) trough with the top 0.23-m (9-in.) raked and compacted between runs. There was no moisture content listed for the sand other than the best dried 'A' classification. Sand cone index values from a Farnell cone penetrometer were obtained on-site and at Bristol University and are shown in Table 5.

Table 6 lists the tire deflections and associated loads. Tests were performed with the tire at 240 kPa (35 psi), and the velocity varied from 1.5 m/s to almost 24.1 m/s (5–79 ft/s) (3–47 knots). There are no footprint areas given for the tire.

The rut depth measurement technique used was thought to be faulty at the higher velocities, and the author felt that that contributed to considerable scatter in the rut depth data. The rut depths were plotted as a sinkage ratio by dividing the rut depth by the undeflected tire diameter.

Table 5
Farnell Cone Index values for the sand described in [7]

| Depth | | Cone index range | |
|---|---|---|---|
| (in.) | (m) | Bristol | Cranfield |
| 0 | 0 | 0 | 0 |
| 3 | 0.0762 | 25–40 | 23–40 |
| 6 | 0.1524 | 66–110 | 48–84 |
| 9 | 0.2286 | 200 (Avg) | 80–222 |

Table 6
Tire deflections and loads from [7]

| Deflection (%) | Load | |
|---|---|---|
| | (lb) | (kN) |
| 30 | 2000–2900 | 9–13 |
| 35 | 4000–4990 | 17.8–22.2 |
| 45 | 4990–6000 | 22.2–26.7 |

The sinkage ratios versus RFF data from the 30% deflection tire show an exponentially rising trend with increasing RFF. The 35% and 45% deflection data appear to be linearly rising with increasing RFF. The shape of our $Z/D$ versus RFF data, shown in Fig. 7 are different when viewed according to sand depth. It appears that our data could fit a linear relationship, given the scatter caused by the velocity effects.

The RFF versus velocity curves shown in Fig. 12 from [7] all have the same general shape, rising to a peak around 6.1 m/s (20 ft/s) (12 knots) and then decreasing, steeply at first, to about 15.2 m/s (50 ft/s) (29 knots), past which they level out. The location and magnitude of the peak RFF vary with tire deflection. The 30% deflection tire has the highest RFF of 0.6 at 6.1 m/s (20 ft/s) (12 knots), the 35% about 0.45 at about 7.6 m/s (25 ft/s) (15 knots), and the 45% deflection peaking at approximately 0.3 at about 4.6 m/s (15 ft/s) (9 knots). The RFF versus velocity data from this study exhibit the same general trends as ours and the RFF values are similar.

## 5. Analytical representation

There have been several attempts at analytical characterizations of soil drag at CRREL [8] regarding aircraft performance from soft surface fields. This report will look at some of those analytical representations to see if they describe the experimental results obtained in this study.

Richmond et al. [11] uses an empirically based approach to predict rut depth and rolling resistance with velocity using a "dynamic mobility number" developed empirically at the US Army's Waterways Experiment Station (WES). This method predicts "dynamic sinkage" through equations that use the WES empirically determined mobility number along with the tire velocity, displacement, and footprint length and the vertical axle displacement. The dynamic mobility number is determined using the material

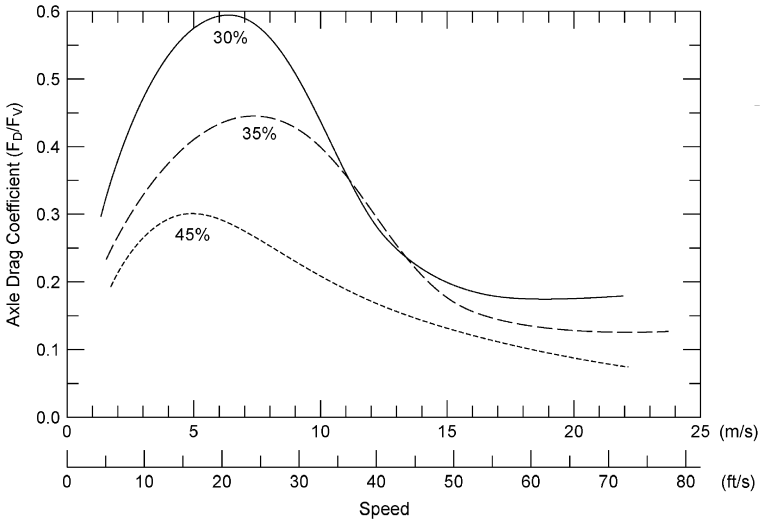


Fig. 12. RFF versus velocity curves from Beaty [7].

Cone Index and the tire velocity and footprint length. (Since this procedure is empirically based, the units need to be as listed below.)

The WES dynamic sand mobility number is defined as:

$$\Omega'_s = \frac{D}{1.6}\frac{G(bd)^{\frac{3}{2}}}{F_v}\left(\frac{\delta_t}{h_t}\right) \tag{4}$$

where $b$ is the tire width in inches, $d$ is the tire diameter in inches, $F_v$ is the load on the tire in pounds, $\delta_t$ is the tire deflection in inches, $h_t$ is the tire section height in inches, $G$ is the average rate of increase in cone index values over a depth equal to the tire width with units of psi/in. $D$, the dynamic factor, is

$$D = 1.0 + 1.34e^{(-1.27t_p)} \tag{5}$$

and $t_p$ is the pulse time defined as:

$$t_p = \frac{l_t}{V} \tag{6}$$

where $l_t$ is the footprint length in inches and $V$ is the tire velocity in in./s. The tire sinkage resulting from the tire at velocity is then defined as the dynamic sinkage $z'$:

$$z' = \left(\frac{0.3439}{\Omega'_s - 0.6239} - 0.0017\right)d. \tag{7}$$

The tire drag is then computed from

$$F_D = \frac{D_T}{F_V}F_v + \frac{1}{2}\rho_s b C_{D_I} z' V^2 \tag{8}$$

where $\frac{D_T}{F_V}$ is the low-speed drag coefficient, $\rho_s$ is sand density, $\frac{1}{2}\rho_s b$ is in the units of lb s$^2$/in.$^3$, and $C_{D_I}$ is an impingement drag coefficient. In $F_D$ the variables before the plus sign constitute a low-speed term, and those after are a high-speed term. $\frac{D_T}{F_V}$ can be written in terms of $\Omega'_s$ and some empirically determined constants in the following form:

$$\frac{D_T}{F_V} = \frac{0.6490}{\Omega'_s - 2.2222} + 0.366. \tag{9}$$

Calculating the drag from Eq. (8) requires knowing $z'$ and $C_{D_I}$. The value of $z'$ must be calculated through an iterative process, since it depends on the velocity and footprint length, which depend on how deep the tire has sunk. The impingement drag coefficient is an empirically determined constant. Richmond assumes it to be proportional to the tire frontal area dynamic soil pressure $q_s$ in psi, where

$$q_s = \frac{1}{2}\rho_s V^2 \tag{10}$$

analogous to slush drag from previous studies. Richmond describes its value as constant with velocity up until planing is initiated, where it then decreases at some linear rate. He suggests that this planing velocity can be calculated with knowledge of another empirically determined constant, the tire lift coefficient, through

$$V_P = \left[\frac{2F_V}{A_t\rho_s C_{L_t}}\right]^{\frac{1}{2}} \tag{11}$$

where $A_t$ is the tire gross footprint area and $C_{L_t}$ is the tire lift coefficient. The tire lift coefficient is defined as

$$C_{L_t} = \frac{2F_V}{A_t\rho_s V_P^2} \tag{12}$$

which is the planing velocity Eq. (11) rearranged. Since the tire lift coefficient is unknown the planing velocity was estimated from the measured data and Fig. 13 from Richmond was used to calculate the $C_{D_I}$.

The dynamic sinkage calculated by Richmond's method and the measured rut depths are compared in Fig. 14. Richmond's method does not have material depth as a variable, and, as Fig. 14 shows, the calculated depths predict what developed in the experimental 0.0508-m (2-in.) deep sand and underpredict what developed in the 0.127-m and 0.1778-m (5 and 7-in.) deep sand. Richmond's predictions are sensitive to the value of $G$ in Eq. (4) above and a lower $G$ will raise the prediction of Rut depth but with no speed

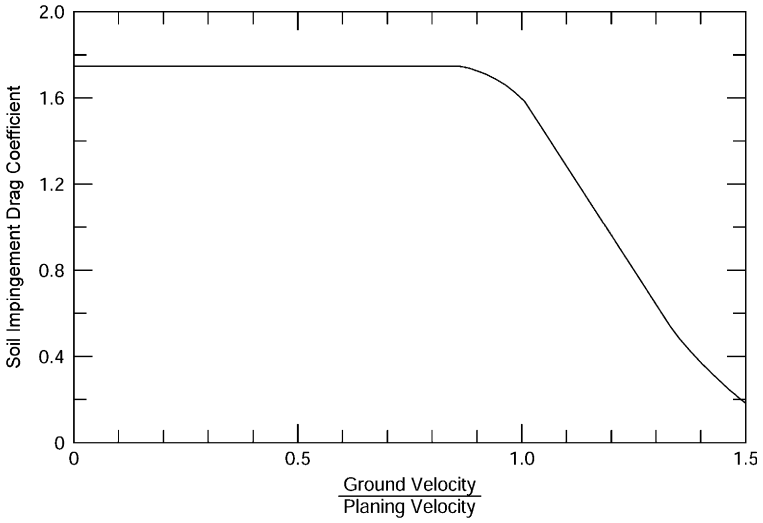


Fig. 13. $C_{D_i}$, Soil impingement drag coefficient, after [11].

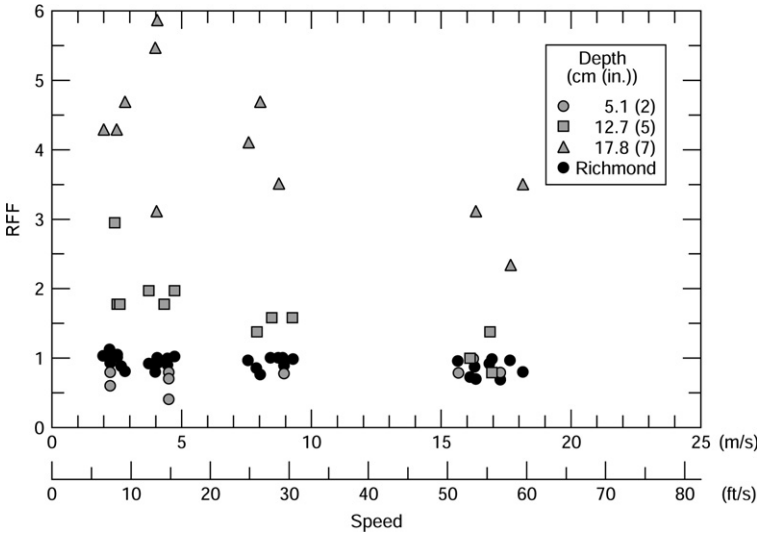


Fig. 14. Experimental rut depths compared with Richmond's predicted rut depths.

or load effect evident. Fig. 15 compares the measured RFF values and those predicted using Eq. (6) to calculate the tire drag forces. Richmond's method overpredicts the 0.0508-m (2-in.) deep sand RFF values even though his rut depth predictions were good with the measured ruts at that depth and underpredicts the 0.127-m (5-in.) deep and 0.1778-m (7-in.) deep sand RFF values as did his rut depth predictions. It generally appears that the trends and estimates from Richmond's method follow the measured data well except for the discrepancies caused by the depth of the loose material.

An attempt was made to correct for this by assuming that the discrepancy was caused by the stress bulb beneath the tire interacting with the solid layer proportional to the ratio of the volume of the interrupted stress bulb to one in an infinitely deep layer of sand. A Boussinesq stress analysis was performed for each nominal load condition and sand depth, and the stress bulb volumes were determined up to where the stress levels were 10% of the surface stress under the tire or to where the bulb intersected the solid layer beneath the sand. This stress bulb volume was then divided by the bulb volume calculated in an infinite layer of sand, and this adjustment was applied to all the predictions. Fig. 16 shows the result of this adjustment.

As can be seen, the adjustment does well at the 0.0505-m (2-in.) depth but underpredicts the RFF values at the 0.127-m (5-in.) and 0.1778-m (7-in.) depths by more than Richmond's original predictions.

The results shown in Fig. 14 might indicate that the error in Richmond's predictions are due to a poor rut depth calculation. To check this, the RFF values were calculated by Richmond's procedures, but the actual rut

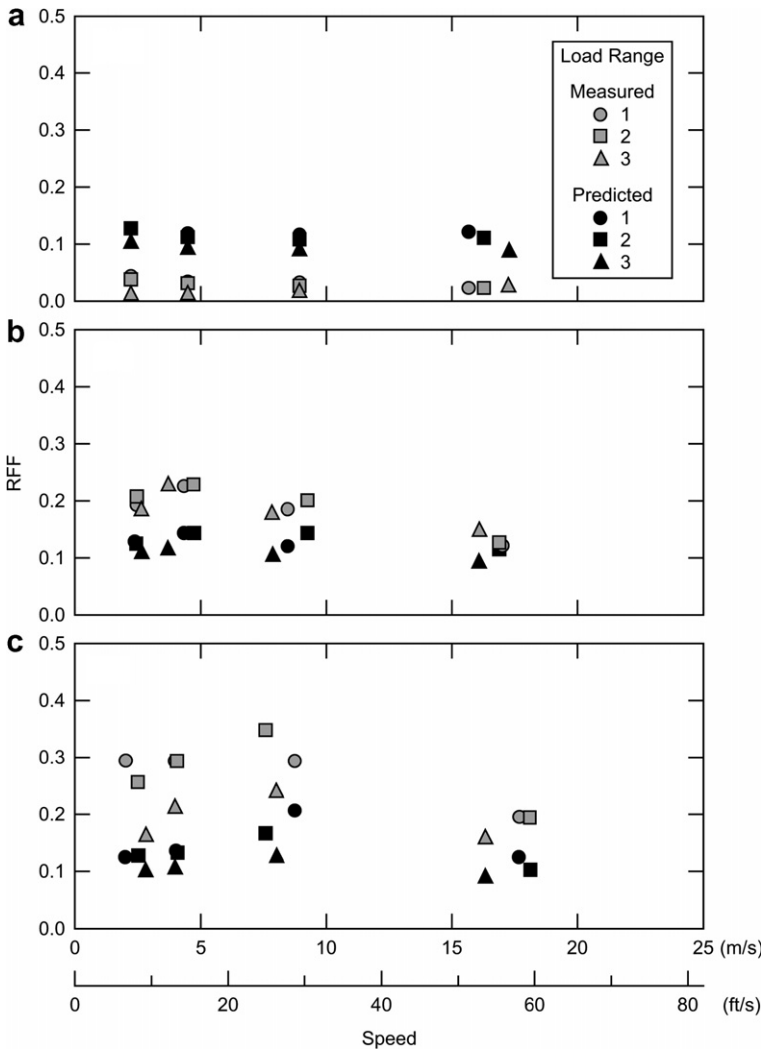


Fig. 15. Measured RFF versus Richmond's predictions for three sand depths, (a) 0.0508 m (2 in.), (b) 0.127 m (5 in.) and (c) 0.1778 m (7 in.).

depth was substituted for the predicted rut depths. The results are shown in Fig. 17. It can be seen that Richmond over predicts all load ranges for the 0.0508-m (2-in.) deep sand and slightly underpredicts the 0.127-m (5-in.) depth sand with the results getting better at the higher speeds. In the 0.1778-m (7-in.) depth Richmond's predictions using the actual rut depths do well in the middle of the velocity range and slightly under predicts at the lowest and highest speeds shown.

The general form of RFF versus speed using Richmond's procedure is shown in Fig. 18 for one load. The form of this relationship depends to a large extent on load and $C_{D_I}$, which depends on the planing velocity. In Fig. 18, $C_{D_I}$ estimated from the measured data determines where the peak in the RFF versus speed curve occurs. The load will shift the magnitude of the curves. The planing velocity in the 0.0508-m (2-in.) deep sand (if any) was estimated to drop quickly from its maximum at low speeds to a very low value, whereas in the 0.127-m (5-in.) and 0.1778-m (7-in.) deep sand, it stays at the maximum value longer and takes longer to approach its minimum value. Since Richmond's method is influenced so greatly by the planing velocity/tire lift coefficient, it is difficult to apply it in a predictive manner without accurately knowing one of those parameters. Another discrepancy is where the low-speed values of the RFF start high and then initially decrease with increasing velocity. We did not notice this trend in our data, perhaps because our lowest speed was not low enough to notice the effect. The solution proposed by Crenshaw [9] and investigated in Shoop et al. [8] is a refinement of Richmond's procedures but suffers from the same limitation relative to $C_{D_I}$.

In the previous CRREL investigations a linear relationship between RFF and speed squared times till depth was noticed across test sites. The data from this set of experiments are presented in Fig. 19 in that form. Here there are linear relationships evident, but the linearity is within velocity ranges, not depth or load. Numerous attempts to linearize the data to one relationship were unsuccessful, including factoring by the stress bulb volume, footprint length, and deflected tire width.

An analytical equation for snow drag developed by van Es [12] was also investigated to describe soil drag. The

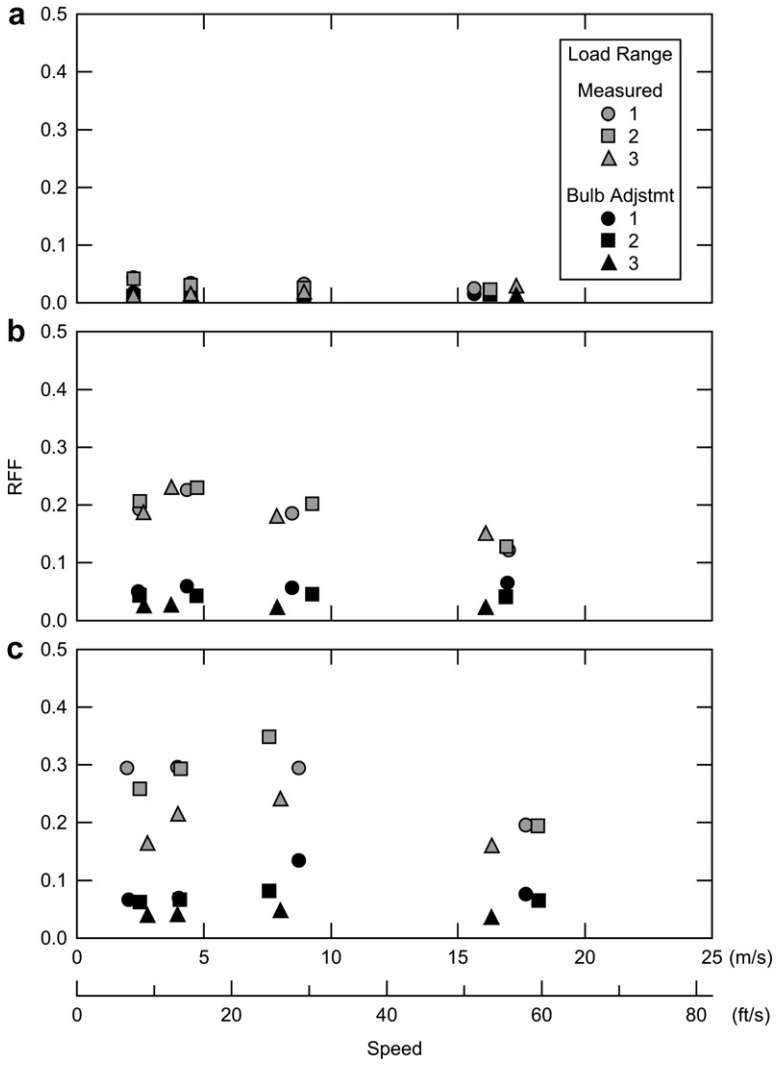


Fig. 16. Measured and stress bulb adjusted RFF, (a) 0.0508 m (2 in.), (b) 0.127 m (5 in.) and (c) 0.1778 m (7 in.) deep sand.

equation parameters needed to apply this to soil were developed, and the results were evaluated in Shoop et al. [8] using data measured by a C-17 aircraft in a fine-grained till. The van Es formulation will be compared here with our sand data below.

Briefly, van Es [12] suggests that the rolling resistance to a high-speed wheel is from two sources: $D_c$, which results from the work needed to compress the material, and $D_d$, from the work necessary to impart dynamic energy to the material to move it vertically. The low speed portion, $D_c$, is related to the sinkage by

$$Z = h_0\left(1 - \frac{\rho_0}{\rho_f}\right) \tag{13}$$

where $h_0$ is the material's initial height, $\rho_0$ is the initial density, and $\rho_f$ is the final density. The low-speed resistance equation is

$$D_c = \frac{w\sigma_i\rho_0 h_0}{\rho_i\sqrt{\lambda}} \int_{u_f}^{u_0} e^{-u^2}\,du \tag{14}$$

where $w$ is the effective tire width, $\sigma_i$ is the strength of ice, $\rho_i$ is the density of ice, $\lambda$ is an empirical value related to the strength of ice, and $u$ is defined as

$$u = \lambda S \tag{15}$$

where $S$ is the void ratio of ice defined as

$$S = \frac{\rho_i}{\rho} - 1 \tag{16}$$

with $\rho$, the material density, equivalent to our $\rho_0$.

$D_d$ is the dynamic portion of the resistance and is defined as

$$D_d = \frac{b}{2}h_0\rho_0 V_g^2\left[\left(1 - \cos^2\alpha_1 - \frac{2}{R}h_f\cos\alpha_1 - \frac{h_f^2}{R^2}\right)\ln\left(\frac{h_0}{h_f}\right) + (h_0 - h_f)\left(\frac{2}{R}\cos\alpha_1 + \frac{2h_f}{R^2}\right) - \frac{1}{2R^2}(h_0^2 - h_f^2)\right.$$

where $b$ is the tire width, $V_g^2$ is the tire velocity, $\alpha_1$ is the angle from vertical to the front of the tire footprint on the ground, $R$ is the tire radius, and $h_f$ is the compacted snow

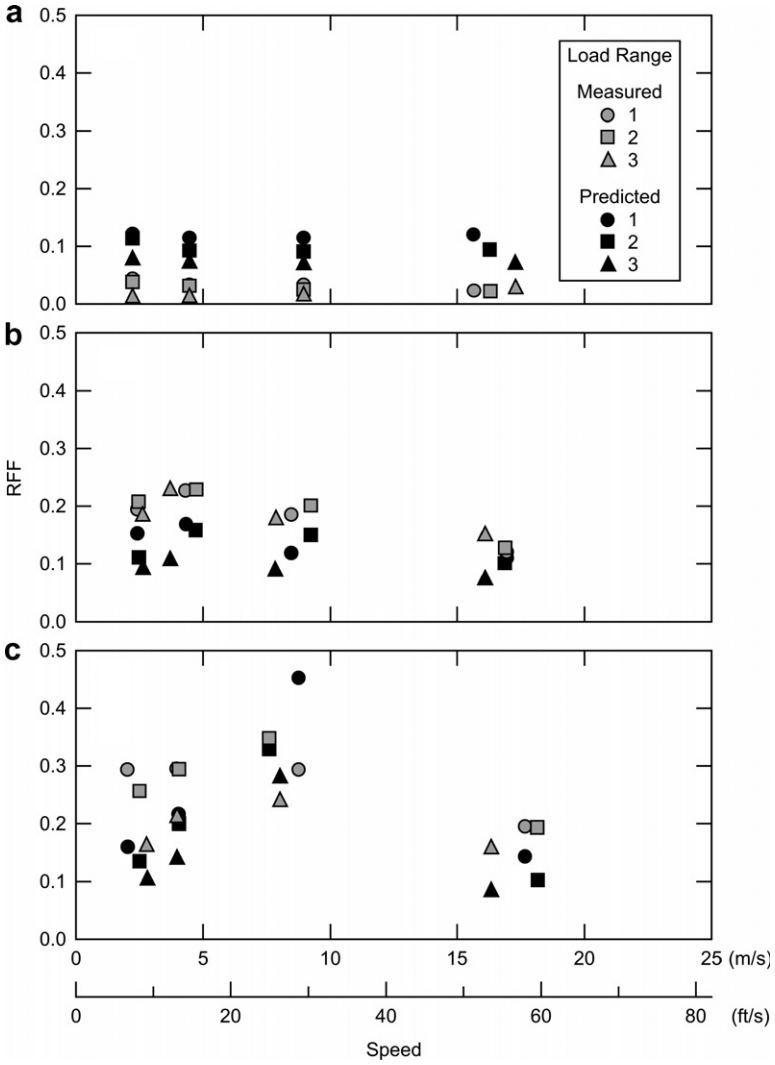


Fig. 17. RFF values calculated by Richmond's method using actual rut depths in three sand depths, (a) 0.0508 m (2 in.), (b) 0.127 m (5 in.) and (c) 0.1778 m (7 in.).

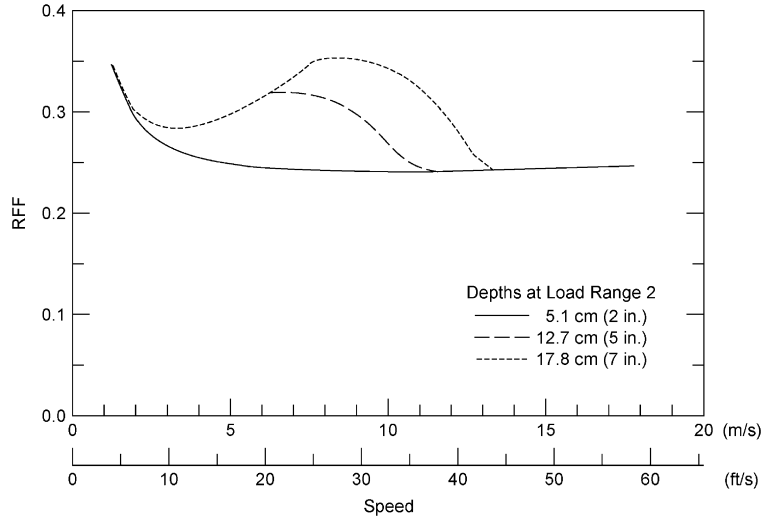


Fig. 18. General form of RFF versus speed calculated using Richmond's method with $C_{D_1}$ estimated from the experimental data.

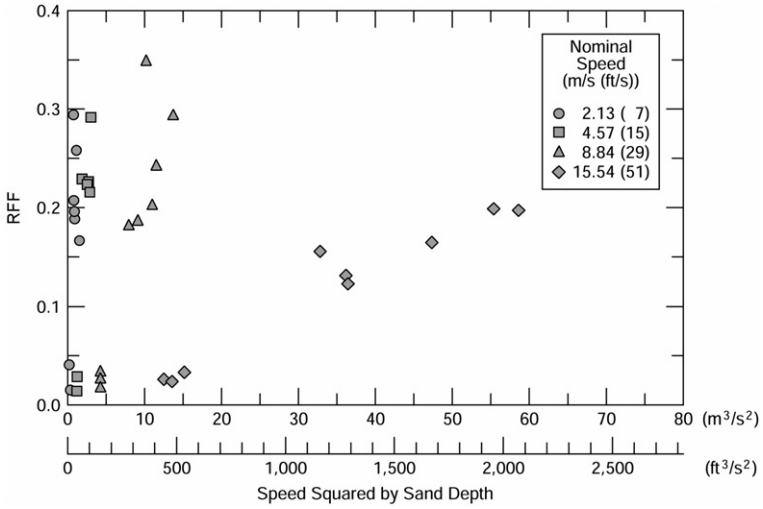


Fig. 19. Measured RFF plotted after Shoop et al. [8].

depth under the rut. The variable $h_f$ is also expressed in terms of our sinkage as

$$h_f = h_0 - Z. \tag{18}$$

The parameters are defined in Fig. 20. More detail on these equations are available in van Es [12].

One of the difficulties in applying the above equations, especially for soil, is in the parameters $\lambda$ and $\rho_f$, which are not known a priori. The solution is sensitive to both these parameters, and their combination can greatly affect the final drag values. Shoop et al. [8] assumed $\lambda$ to be 6 for the fine-grained till solutions with $\rho_f$ equal to 1922 kg/m$^3$, and those values were used in the following calculations. Other values were as measured and listed above.

The ruts calculated from Eq. (2) change only with initial till depth with no velocity effect. Applying it to our data gives the results shown in Fig. 21. It can be seen that the rut depth is reasonable for the 0.0508-m (2-in.) deep sand where the undeflected layer is close and the rut does not change much with speed. At the 0.127-m (5-in.) depth the calculated rut is reasonable at the low velocities but overestimates the depth at the highest velocity. However, in the 0.177-m (7-in.) deep sand the calculated rut depth is less than the actual at all but the highest velocity, when the tire is planing and the actual rut decreases to the calculated. Since the rut depths are not estimated correctly under the Van Es method, his resistance equations were applied to our data using the measured rut depths. Fig. 22 shows the RFF values calculated by using Van Es's approach with the actual rut depths from our experiments.

As the figures show, the Van Es approach gives reasonable values for the 0.0508-m (2-in.) deep sand except at the highest velocity, where it underestimates the RFF. In the 0.127-m (5-in.) deep sand it generally underestimates the RFF, approaching the measured at the highest speed where the tire is planing. The one exception is in load range 1 at the slowest speed, where it is much higher than the measured RFF. In the 0.1778-m (7-in.) deep sand in load range 1 it is higher than the measured at all speeds, does well in the mid-speeds with load ranges 2 and 3, and then overpredicts the RFF at the highest speed, where the tire is in a fully developed plane.

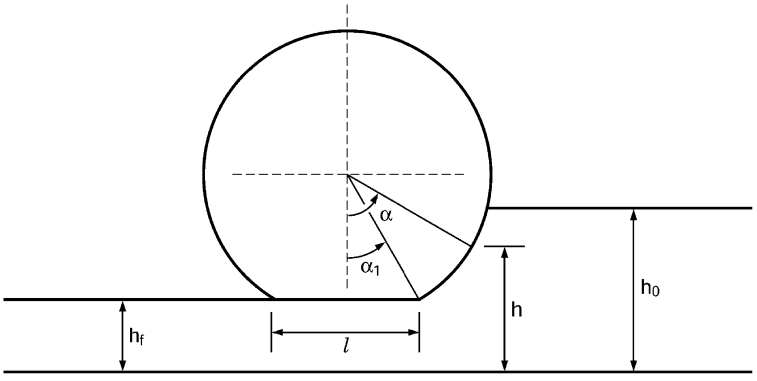


Fig. 20. Physical detail for Van Es equation.

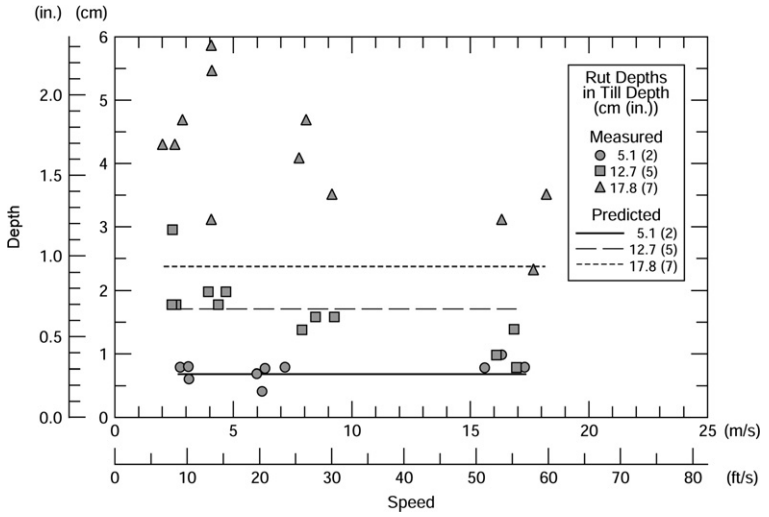


Fig. 21. Measured versus Van Es's calculated rut depths.

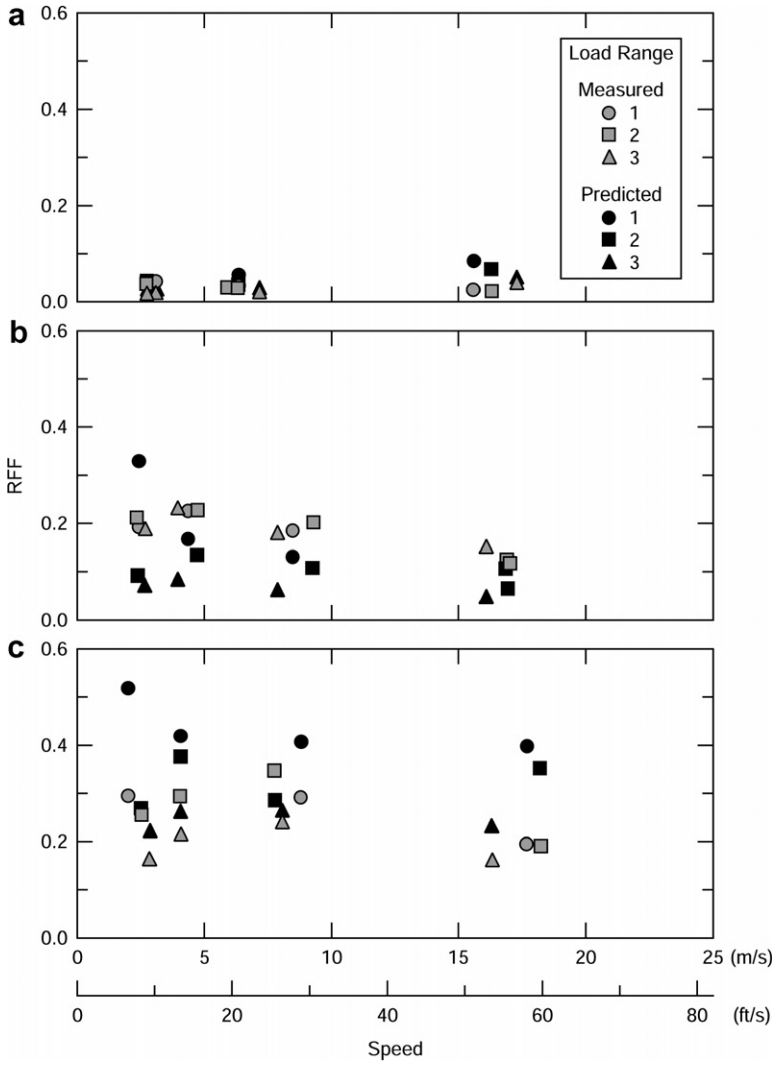


Fig. 22. Measured and Van Es's RFF values for three sand depths, (a) 0.0508 m (2 in.), (b) 0.127 m (5 in.) and (c) 0.1778 m (7 in.).

## 6. Conclusions and recommendations

The experiments performed here show a relationship between sinkage ratio (or in these tests, rut depth) and RFF. They also show a relationship between rut depth and/or RFF and loose material depth, tire load, and velocity. The rut depth that develops depends on the depth of loose surface material present and the dynamics of how that material behaves under the applied strain rate. In addition to velocity (rate of application) and material depth, this is probably also related to the surface area of the tire footprint and the load on the tire, i.e. the applied pressure. We speculate that since our attempts to relate rut depth to the static stress bulb volume were unsuccessful, the applied stress is being dissipated in the near-surface material due to intergranular friction of the sand particles. This is an area that needs further investigation.

We do not see a velocity-squared relationship between RFF and velocity as some previous investigators did, perhaps due to tire planing and the kinetic energy in spray formation.

When our experimental results are compared to previous work, it seems that material type plays a greater role than has been discussed. The previous work has been predominately with cohesive fine-grained clays, which react differently under dynamic loading than the non-cohesive sand used in these experiments. Additionally the sand used in these experiments was dry, and material containing moisture will react differently than a dry material due to the behavior of the pore water and the material's change in response due to the presence of the moisture.

The work discussed here by Richmond et al. [11] follows the form of our data, but it would be difficult to use as a predictive tool, especially with its reliance on the empirical tire lift coefficient, which is not well defined and thus difficult to determine for other tires and load. The shape of the RFF versus velocity curves can be altered to fit the data by adjusting the tire lift coefficient and parameters. Also, that work did not account for the effect of load and material depth, and the tire lift coefficient was changed to account for varying material strength.

We see the need for a better definition of the dynamic response of non-cohesive dry sand to an impulsively applied pressure. It would also be helpful to gather data on the effect of tire diameter and width to incorporate those parameters into an appropriate predictive model.

## Acknowledgments

The author thanks Byron Young of USACRREL and Thomas Yager and his team at NASA Langley Research Center for performing the sand rolling resistance field experiments presented in this report.

## References

[1] Blaisdell, George L, et al. Wheels and tracks in snow, validation study of the CRREL shallow snow mobility model. CRREL report 90-9. Hanover, NH: US Army Cold Regions Research and Engineering Laboratory; 1990.
[2] Richmond, Paul W. Motion resistance of wheeled vehicles in snow. CRREL report 95-7. Hanover, NH: US Army Cold Regions Research and Engineering Laboratory; 1995.
[3] Pope RG. The effect of wheel speed on rolling resistance. J Terramech 1971;8(1):51–8. Pergamon Press.
[4] Turnage, Gerald W. Mobility numeric system for predicting in-the-field vehicle performance, report 1, historical review, planned development. Prepared for US Army Corps of Engineers, miscellaneous paper GL-95-12; 1995.
[5] Crenshaw BM. Soil/wheel interaction at high speed. Automotive Engineering Congress, Detroit, MI; January 11–15, 1971.
[6] Leland, Trafford JW, Eunice G. Smith. Aircraft tire behavior during high-speed operations in soil. NASA technical note TN D-6813; 1972.
[7] Beaty I. An investigation into the rolling resistance if a full size meteor wheel in dry Leighton Buzzard sand using the heavy load friction vehicle. DRIC-BR-49447, S&T Memo 6-75, 1975. Procurement Executive, Ministry of Defense, DA Mech, UK.
[8] Shoop Sally, Richmond PW, Eaton RA. Estimating rolling friction of loose soil for aircraft takeoff on unpaved runways. ERDC/CRREL TR-01-11. Hanover, NH: US Army Cold Regions Research and Engineering Laboratory; 2001.
[9] Crenshaw BM. Aircraft landing gear dynamic loads induced by soil landing fields, vol. 1, June 1972. US Air Force Flight Dynamics Laboratory, Air Force Systems Command, Wright-Patterson AFB, Ohio.
[10] Selig ET, Wang C-T. Effect of velocity on drag and sinkage of free-rolling tires on soil. In: International society for terrain-vehicle systems, 5th international conference; 1975.
[11] Richmond LD, Brueske NW, Debord KJ et al. Aircraft dynamic loads from substandard landing sites, Part II, development of tire-soil mathematical model. AFFDL-TR-67-145, Part II. US Air Force Flight Dynamics Laboratory, Air Force Systems Command, Wright-Patterson AFB, Ohio; 1968.
[12] Van Es GWH. Rolling resistance of aircraft tires in dry snow. National Aerospace Laboratory NLR, NLR-TR-98165; 1998.